Solution Structure of an O^6-[4-oxo-4-(3-Pyridyl)butyl]guanine Adduct in an 11mer DNA Duplex: Evidence for Formation of a Base Triplex†

Lisa A. Peterson,§ Choua Vu,§ Brian E. Hingerty,|| Suse Broyde,⊥ and Monique Cosman*,#

Division of Environmental and Occupational Health and Cancer Center, University of Minnesota, Minneapolis, Minnesota 55455, Life Sciences Division, Oak Ridge National Laboratory, Oak Ridge, Tennessee 37831, Biology Department, New York University, New York, New York 10003, and +*Biology and Biotechnology Research Program, Lawrence Livermore National Laboratory, Livermore, California 94551*

Received July 10, 2003; Revised Manuscript Received September 17, 2003

ABSTRACT: The pyridyloxobutylating agents derived from metabolically activated tobacco-specific nitrosamines can covalently modify guanine bases in DNA at the O^6 position. The adduct formed, O^6-[4-oxo-4-(3-pyridyl)butyl]guanine ([POB]dG), results in mutations that can lead to tumor formation, posing a significant cancer risk to humans exposed to tobacco smoke. A combined NMR−molecular mechanics computational approach was used to determine the solution structure of the [POB]dG adduct within an 11mer duplex sequence d(CCATAT-[POB]G-GCCC)·d(GGGCCATATGG). In agreement with the NMR results, the POB ligand is located in the major groove, centered between the flanking 5′-side dT·dA and the 3′-side dG·dC base pairs and thus in the plane of the modified [POB]dG·dC base pair, which is displaced slightly into the minor groove. The modified base pair in the structure adopts wobble base pairing (hydrogen bonds between [POB]dG(N1) and dC(NH4) amino proton and between [POB]dG-(NH2) amino proton and dC(N3)). A hydrogen bond appears to occur between the POB carbonyl oxygen and the partner dC's second amino proton. The modified guanine purine base, partner cytosine pyrimidine base, and POB pyridyl ring form a triplex via this unusual hydrogen-bonding pattern. The phosphodiester backbone twists at the lesion site, accounting for the unusual phosphorus chemical shift differences relative to those for the control DNA duplex. The helical distortions and wobble base pairing induced by the covalent binding of POB to the O^6-position of dG help explain the significant decrease of 17.6 °C in melting temperature of the modified duplex relative to the unmodified control.

DNA alkylating agents are a large group of diverse chemicals that have long been known to cause mutations, cancer, cell death, chromosome damage, inhibition of synthetic pathways, cell cycle arrest, and teratogenicity in laboratory model systems (*1*). Concerns have been raised about their potential roles in human carcinogenesis since some of these alkylating agents, or their metabolic precursors, have been found to be prevalent in the environment. In particular, the tobacco-specific nitrosamines 4-(methylnitrosamino)-1-(3-pyridyl)-1-butanone (NNK) and *N*-nitrosonornicotine (NNN) are potent carcinogens in laboratory animals and potentially in humans exposed to cigarette smoke (*2*). Both NNK and NNN can be metabolized to pyridyloxobutylating agents, which can covalently bind to DNA (*2*). One pyridyloxobutyl DNA adduct is O^6-[4-oxo-4-(3-pyridyl)-butyl]guanine ([POB]dG),[1] Figure 1) (*3*).

The [POB]dG adduct has recently been observed in liver DNA of mice treated with NNK (*5*) and can serve as a substrate for repair by O^6-alkylguanine-DNA alkyltransferase (*3*−*5*). If not repaired, this adduct is highly mutagenic in both human kidney cells and *Escherichia coli* strain BH10B (*6*). In *E. coli*, the [POB]dG adduct produced exclusively G → A transition mutations, while in the human kidney cells, the mutation spectrum was much more complex; G → A transition mutations predominate, but other types of mutations were also observed, including G → T transversions, deletions, and compound and remote mutations (*6*).

The alkylation of the O^6 position of the guanine alters its hydrogen-bonding possibilities because the N1 position no longer has a proton (Figure 1). Thus, this nitrogen becomes a potential hydrogen-bonding acceptor rather then a donor. Several base pairing schemes have been observed experimentally for the O^6-methyl-dG (O^6meG) and O^6-ethyl-dG (O^6etG) adducts when paired with other bases in DNA (*7*, *8*), and similar possibilities for the [POB]dG·dC base pair are likely (Figure 2). The type shown in Figure 2a would

† Supported by grants from the NIH (CA59887 (L.A.P.) and CA75449 (S.B.)) and by ORNL Laboratory Directed Research and Development funding (B.E.H.).

‡ Structure coordinates have been deposited with the Protein Data Bank (http://www.rcsb.org.pdb) (PDB code 1PYJ).

* To whom correspondence should be addressed. Phone: (925) 423-1647. Fax: (925) 424-3130. E-mail: cosman1@llnl.gov.

§ University of Minnesota.

|| Oak Ridge National Laboratory.

⊥ New York University.

Lawrence Livermore National Laboratory.

[1] Abbreviations: [POB]dG, O^6-[4-oxo-4-(3-pyridyl)butyl]guanine; [POB]dG·dC 11mer duplex, d(CCATAT-[POB]G-GCCC)·d(GGGCCATATGG); O^6meG, O^6-methyl-dG; O^6etG, O^6-ethyl-dG; NOE, nuclear Overhauser effect; NOESY, nuclear Overhauser effect spectroscopy; ROESY, rotational Overhauser effect spectroscopy; COSY, correlated spectroscpy; TOCSY, total correlated spectroscopy.

10.1021/bi035217v CCC: $25.00
Published on Web 10/22/2003

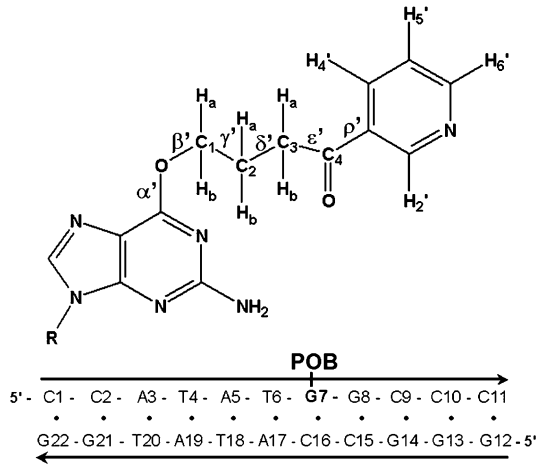

FIGURE 1: Schematic structure of the O^6-[4-oxo-4-(3′-pyridyl)butyl]-guanine adduct ([POB]dG7) and the numbering scheme for the DNA 11mer sequence. The POB to dG linkage is defined by torsion angles $\alpha' =$ [POB]dG7(N1)-[POB]dG7(C6)-[POB]dG7(O^6)-POB(C1) and $\beta' =$ [POB]dG7(C6)-[POB]dG7(O^6)-POB(C1)-POB(C2). The angles in the POB oxobutyl chain are defined by torsion angles $\gamma' =$ [POB]dG7(O^6)-POB(C1)-POB(C2)-POB(C3), $\delta' =$ POB(C1)-POB(C2)-POB(C3)-POB(C4), and $\epsilon' =$ POB(C2)-POB(C3)-POB(C4)-POB(C3′). The rotation of the pyridyl ring with respect to the chain is defined by the torsion angle $\rho' =$ POB(C3)-POB(C4)-POB(C3′)-POB(C4′).

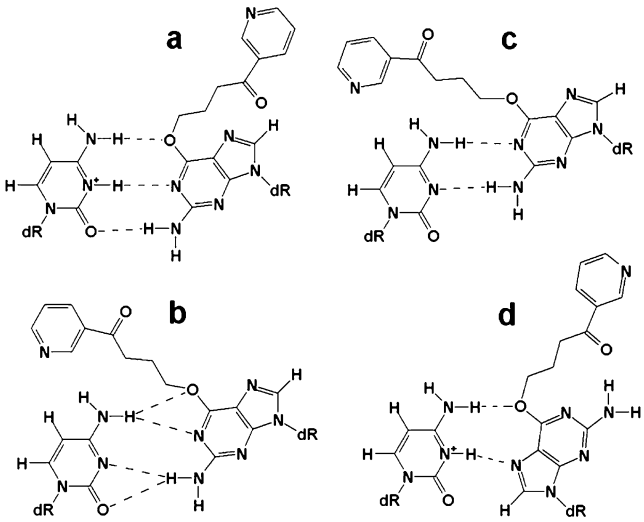

FIGURE 2: Possible hydrogen-bonding schemes for the [POB]dG·dC base pair: (a) protonated cytosine opposite [POB]dG with the POB ligand proximal (pointing toward N7); (b) bifurcated hydrogen bonding with the POB ligand distal (pointing away from N7); (c) wobble hydrogen bonding; and (d) cytosine protonated and [POB]-dG in syn orientation. The pyridyl ring can also adopt two different orientations with respect to the carbonyl group in the aliphatic chain: having the nitrogen on the same side, as in panel d, or on opposite sides, as in panels a−c.

require a protonated cytosine, which has been previously observed in the Z-DNA crystal structure of a DNA oligomer containing an O^6meG·dC base pair (*9*) and in an NMR study of an O^6meG·dC nucleoside base pair in chloroform (*10*). The bifurcated hydrogen-bonding scheme shown in Figure 2b has been observed for one of two O^6etG·dC base pairs in the crystal structure of a self-complementary duplex stabilized by minor groove binding drugs (*8*). The second O^6etG·dC base pair adopted a wobble-bonding scheme as shown in Figure 2c (*8*). A wobble type hydrogen bonding (Figure 2c) was also proposed for an O^6meG·dC base pair in an NMR study of a modified DNA duplex (*11*). Hoogsteen base pairing can occur if either the modified or the partner base adopts a syn orientation about the glycosidic torsion angle (Figure 2d); this has been observed for the modified guanine in the NMR structure of an O^6meG·dG base pair mismatch (*12*) and in the crystal structure of an O^6meG·dA base pair mismatch in modified DNA duplexes (*9*).

In comparison to the O^6meG and O^6etG adducts, the [POB]dG adduct would be expected to pose a greater challenge in structural determination. There are greater degrees of freedom of rotation due to a longer butyl chain and pyridyl ring, which can interact with the DNA nonspecifically, resulting in a heterogeneous mixture consisting of a number of conformers. The [POB]dG or partner cytosine may adopt either a syn (e.g., Figure 2d) or anti glycosidic torsion angle relative to its sugar. The POB can orient either in a distal (pointing away from N7) or proximal (pointing toward N7) conformation (Figure 2). The carbonyl oxygen and pyridyl ring nitrogen are potential hydrogen-bond acceptors, and the pyridyl ring may or may not intercalate into the DNA. Yet, despite these expected challenges, it was possible to determine a single conformation for the [POB]-dG adduct within an 11mer duplex sequence d(C1-C2-A3-T4-A5-T6-[POB]G7-G8-C9-C10-C11)·d(G12-G13-G14-C15-C16-A17-T18-A19-T20-G21-G22) (Figure 1). A combined NMR−molecular mechanics computational approach was used to provide a detailed structural view of the types of distortions that can be induced into DNA by a bulky and flexible alkylating agent, such as POB, at the O^6 position of guanine.

MATERIALS AND METHODS

Preparation of the Duplex Adduct. 5′-*O*-(4,4′-Dimethoxytrityl-N^2-phenoxyacetyl)-O^6-{3-[2-(3-pyridyl)-1,3-dithian-2-yl]propyl}-2′deoxyguanosine-3′-*O*-(2-cyanoethyl)-*N*,*N*-diisopropylamide-*O*-phosphite was prepared as described previously (*4*). The 11mer oligodeoxyribonucleotide 5′-CCATATG*GCCC, where G* = O^6-{3-[2-(3-pyridyl)-1,3-dithian-2-yl]propyl}-2′-deoxyguanosine, was synthesized by Oligos Etc. (Wilsonville, OR). The oligomer was released from the solid support upon heating in concentrated ammonium hydroxide at 55 °C overnight. The supernatant was concentrated to dryness under reduced pressure, and the residue was redissolved in 100 mM ammonium acetate (1 mL). The oligomer containing dithiane-protected O^6-[POB]-dG was eluted from an ODS Hypersil column (Keystone Scientific, Inc., Bellfonte, PA) with a 30 min linear gradient from 100 mM ammonium acetate containing 5% acetonitrile to 100 mM ammonium acetate containing 20% acetonitrile (*4*). Oxidative removal of the dithiane group was accomplished by treating the 11mer with a 5-fold excess of *N*-chlorosuccinimide in aqueous acetonitrile (*4*). After 40 min, the reaction was diluted with 100 mM ammonium acetate (0.8 mL), and the reaction mixture was separated on a Phenomenex C18 Bond-clone column (Phenomenex, Torrence, CA). The product was eluted with a 30 min linear gradient from 100 mM ammonium acetate containing 5% acetonitrile to 100 mM ammonium acetate containing 20% acetonitrile (retention times: unmodified oligomer, 17 min; oligomer containing [POB]dG, 21.5 min; and oligomer containing dithiane-protected [POB]dG, 26.3 min). The oligomer containing [POB]dG was further purified using the

Hypersil column (see previously, eluted as a single peak at 16.5 min), and the adduct identity was verified by both enzymatic hydrolysis with snake venom phosphodiesterase and mass spectrometric analysis, as described previously (*6*). The modified 11mer strand was annealed to its complementary strand at 70 °C, and the stoichiometry was followed by monitoring the ratio of resolved single proton NMR resonances belonging to each strand.

UV Melting Experiments. Melting curves were acquired by measuring the changes in absorption at 260 nm using an Agilent 8453 UV−vis spectrophotometer equipped with an Agilent 89090A Peltier heat controller. All melting curves were measured with solutions of oligomers that had an initial absorbance of 0.3−0.5 at 260 nm at 20 °C in 20 mM sodium phosphate, 0.2 M NaCl, and 0.2 mM EDTA, pH 7. The temperature was increased at a rate of 0.5 °C/min. Each experiment was run three times, and an average of the melting temperature ($T_m \pm$ standard deviation) was recorded.

NMR Experiments. NMR experiments were performed on a Varian INOVA 600 MHz spectrometer. A combination of through space nuclear and rotational Overhauser effect spectroscopy (50 and 300 ms mixing time NOESY and 100 ms spin lock time ROESY, respectively,) and through bond correlated and total correlated spectroscopy (phase-sensitive COSY and 40 and 80 ms spin lock time TOCSY, respectively) experiments were recorded in the States-TPPI mode on approximately 5 mg of the [POB]dG·dC 11mer duplex (and 7 mg of the control 11mer duplex) dissolved in 0.6 mL of D_2O buffer (10 mM Na_2PO_4, 0.1 M NaCl, 0.1 mM EDTA, pH 7.0) at 25 and 5 °C. The temperature of the sample was calibrated with an external methanol sample. 1-D and NOESY (150 ms mixing time) spectra of the adduct duplex in 90% H_2O/10% D_2O buffer were collected at 5 °C using a jump−return pulse sequence for solvent suppression. Sweep widths of 6000 and 12 000 Hz were used for the adduct duplex dissolved in D_2O buffer and H_2O buffer, respectively, with 1024 or 2048 complex data points and 300 t_1 increments, each having either 32 or 64 transients and a recycle delay of 1.8 s. The indirect proton−phosphorus correlation (*13*) spectra were acquired on the [POB]dG·dC and control 11mer duplexes in D_2O at 25 and 5 °C and referenced relative to external 10% trimethyl phosphate. Sweep widths of 3600.8 and 1457.7 Hz were used for the ^1H and ^{31}P dimensions, respectively, with 1024 complex data points and 128 t_1 increments, each having 128 transients and a recycle delay of 1.3 s. Natural abundance ^{13}C-carbon-proton heteronuclear multiple quantum coherence (HMQC) spectra were recorded in D_2O buffer at 25 and 5 °C. The proton carrier frequency was set on the water resonance with a sweep width of 10 ppm, and the ^{13}C carrier frequency was set to 75 ppm with a sweep width of 150 ppm. The carbon spectra were referenced relative to external 3-(trimethylsilyl)-propionate using the method described by Bax and Subramanian (*14*). Data sets were processed using the software package VNMR (Varian Inc, Palo Alto, CA) and transferred to a SGI workstation, and the phase file was converted directly into FELIX (Accerlys, San Diego, CA) matrixes for analysis.

Several factors went into the conversion of the NOE cross-peak volumes into the distance bounds used for the structure determination of the adduct duplex. Distance restraints involving nonexchangeable protons were estimated from the volume buildup curves measured from a set of 40, 80, 120, 160, and 200 ms mixing time NOESY experiments at 5 °C. Either the fixed 2.45 Å dC(H6) to dC(H5) distance or the averaged fixed 3.06 Å dT(H6) to dT(CH_3) distance (for proton to methyl group distances) was used in the two spin approximation calculations for obtaining the DNA−DNA distance restraints. DNA−DNA distance restraints were not obtained for the exchangeable protons due to overlapped and broad resonances. Because the resonances that correspond to the POB ligand and the modified base pair are also broad and/or overlapped, the DNA−POB distance bounds were estimated by the number of contour levels as very weak (4.5−6.0 Å), weak (3.8−5.5 Å), medium-weak (3.3−5.0 Å), medium (2.8−4.5 Å), medium-strong (2.3−4.0 Å), and strong (1.8−3.5 Å). The estimation also took into account whether the corresponding NOE cross-peak involved single protons, a methyl group, or an average of two or more protons.

The proton−proton vicinal coupling constants for the sugar protons were analyzed from phase-sensitive COSY spectra to qualitatively distinguish between C3′-endo and C2′ endo family of sugar puckers. The relative intensity of the NOE cross-peaks between the base protons and their own and 5′ flanking sugar H2′, H2″, and H3′ protons was used to qualitatively distinguish between the A and the B family of helices for the modified duplex (*15*).

Molecular Mechanics Computations. Restrained conformational searches were carried out with DUPLEX, a molecular mechanics program that has been especially tailored for investigating the conformations of carcinogen−nucleic acid adducts. Key features of DUPLEX are that it employs a consistent force field for both the carcinogen and the DNA and that the potential energy minimizations are performed in the reduced variable domain of torsion angle space (*16*). Full details of this approach are given in earlier work (*17*). Parameters, namely, partial charges (Supplementary Information, Table S1) and optimized geometry, for the [POB]dG adduct were determined using the program Guassian98 (http://www.Gaussian.com/) (*18*). Gaussian98 together with the CNDO method was also used to obtain bond lengths, bond angles, and dihedral angles for the POB ligand by geometry optimization of a model originally built with standard parameters. Thirty-two energy minimization trials were carried out for a 5 base pair segment of the adduct duplex: d(A5-T6-[POB]dG7-G8-C9)·d(G14-C15-C16-A17-T18). Each run uses a minimal set of NOE-derived distance restraints, together with information from the NMR data on the hydrogen-bonding pattern, and with initial linkage torsion angles (Figure 1) α' and β' at 0, 90, 180, and 270° and ρ' at 0 and 180°, in all combinations. The remaining angles (Figure 1) were started at 180° (extended configuration) but were not restrained. The torsion angle barriers employed are given in Table S2 (Supporting Information). All glycosidic torsion angles were started in the anti domain ($\chi = 240°$), with the exception of the [POB]dG residue, which was initially started either in the anti or in the syn domain ($\chi = 60°$). Having the modified guanine syn did not agree with the NMR data; thus, in all subsequent runs, χ for the [POB]-dG residue was started in the anti domain. The DUPLEX hydrogen-bond penalty function was employed for Watson−Crick base pairing at all residues except for [POB]dG7·dC16, in line with the NMR data. In the initial runs, the [POB]-

dG7·dC16 base pair either had no hydrogen-bonding restraints or had two of the three standard Watson−Crick hydrogen-bonding restraints (C16 amino to [POB]dG7 O^6 and C16 O^2 to [POB]dG7 amino). None of the structures with the Watson−Crick hydrogen-bonding restraints converged, while several of the structures with no hydrogen-bonding restraints adopted the wobble base pairing scheme shown in Figure 2c. Thus, the following two hydrogen-bonding restraints were added to subsequent runs: C16 amino to [POB]dG7 N1 and C16 N3 to [POB]dG7 amino. An additional POB−DNA hydrogen-bond was added as a restraint in the final runs, in agreement with the NMR data. The pyridyl ring can rotate with respect to the butyl chain (dihedral angle ρ' in Figure 1), and it exhibits only one very weak NOE contact with the dT6 methyl group, so it was not possible to unambiguously determine a single orientation for this aromatic ring.

The resulting 5mer adduct duplex structures were ranked according to energy and goodness of fit to the NOE restraints. At this point, the set of NMR assigned distance bounds were evaluated in relation to achieved distances and energies in the ensemble of 32 structures. The 10 structures with the best agreement to the NOE restraints and having the lowest energies were then built to the larger 11mer modified duplex with all restraints included. A total of 298 NOE distant restraints (271 DNA−DNA, 5 POB−POB, and 22 DNA−POB) and 29 hydrogen-bonding restraints were employed in the final runs. Helical parameters were calculated using the nucleic acid structure analysis program 3DNA (*19*, *20*), and ball-and-stick figures of a representative structure were generated using Molscript VI.1 (*21*).

RESULTS AND DISCUSSION

UV Melting Studies. To determine the effect of the [POB]-dG adduct on the stability of the DNA double helix, the thermal melting curves for the [POB]dG·dC 11mer duplex and the control unmodified 11mer duplex were obtained (Supporting Information, Figure S1). When [POB]dG is opposite dC, the double stranded oligomer melts at much lower temperatures than the unmodified duplex (T_m = 35.1 ± 1.0 vs 52.7 ± 0.9 °C, respectively (ΔT_m = 17.6 °C)), indicating that the formation of the [POB]dG adduct is significantly destabilizing to duplex DNA. Similar destabilization of duplex DNA was observed when modified with the simpler O^6-alkylguanine adducts (*22*).

NMR Resonance Assignment and Chemical Shift Studies. NMR data used for the structural calculations were collected at 5 °C to help narrow the line widths of the cross-peaks belonging to the POB ligand and the modified [POB]dG7·dC16 base pair. Lowering the temperature decreases the motional flexibility inherent in the POB ligand. The nonexchangeable proton chemical shifts belonging to POB and [POB]dG7·dC16 did not change significantly upon going from 25 to 5 °C (Table S3) and suggest that the signal broadness results from the degrees of freedom in rotation about bonds in the butyl chain of the POB ligand rather than to the presence of multiple conformations.

The NOE connectivities between POB−POB protons, POB−DNA protons, and DNA−DNA protons are designated in the plots of the regions of the 300 and 150 ms mixing time NOESY spectra at 5 °C of the [POB]dG·dC adduct duplex dissolved in D_2O and H_2O buffer, respectively (Figures 3 and 4). Standard nucleic acid assignment procedures were used to assign the DNA protons (*23*, *24*). The assignments for the nonexchangeable and exchangeable DNA protons are given in the Supporting Information, Tables S4 and S5, respectively.

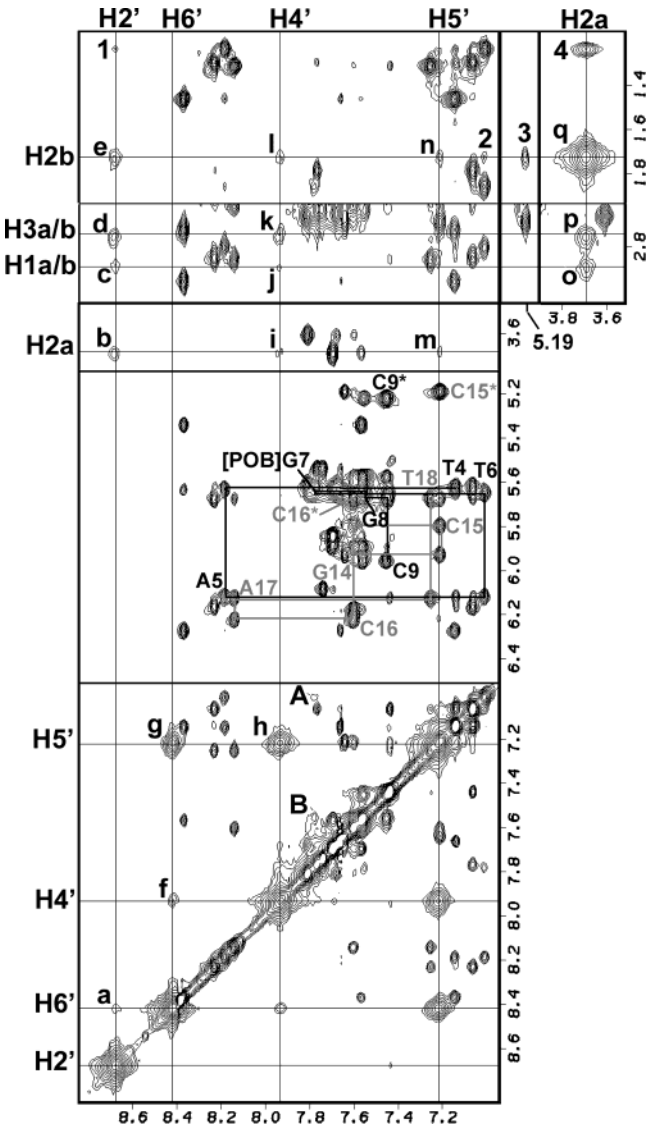

FIGURE 3: Expanded tiled regions of the 300 ms NOESY spectrum at 5 °C of the [POB]dG·dC 11mer duplex in D_2O buffer. The NOE connectivities between the base protons and their own and 5′ flanking sugar H1′ protons are designated for the modified strand from dT4 to dC9 (black lines) and for the complementary strand from dG14 to dT18 (gray lines). NOEs between [POB]G7(H8) and G8(H8) (peak A) and T6(H6) (peak B) indicate that the modified guanine is stacked within the helix. The cytosine H5 to H6 NOEs for C9, C15, and C16 are designated by *. The intramolecular connectivities between POB resonances (intersection of light gray lines) are designated by a−q and assigned as follows: a−e, H2′ to H6′, H2a, H1a/b, H3a/b, and H2b, respectively; f and g, H6′ to H4′ and H5′, respectively; h−l, H4′ to H5′, H2a, H1a/b, H3a/b, and H2b; m and n, H5′ to H2a and H2b, respectively; and o−q, H2a to H1a/b, H3a/b, and H2b, respectively. Four intermolecular connectivities between POB and major groove DNA protons are labeled by numbers as follows: 1, POB(H2′) to T6(CH_3); 2, T6(H6) to POB(H2b); 3, POB(H2b) to C15(H5); and 4, POB(H2a) to T6(CH_3).

The DNA base to sugar H1′ connectivities can be readily followed along the modified strand segment d(T4-A5-T6-[POB]dG7-G8-C9) (black lines, Figure 3), with the exception

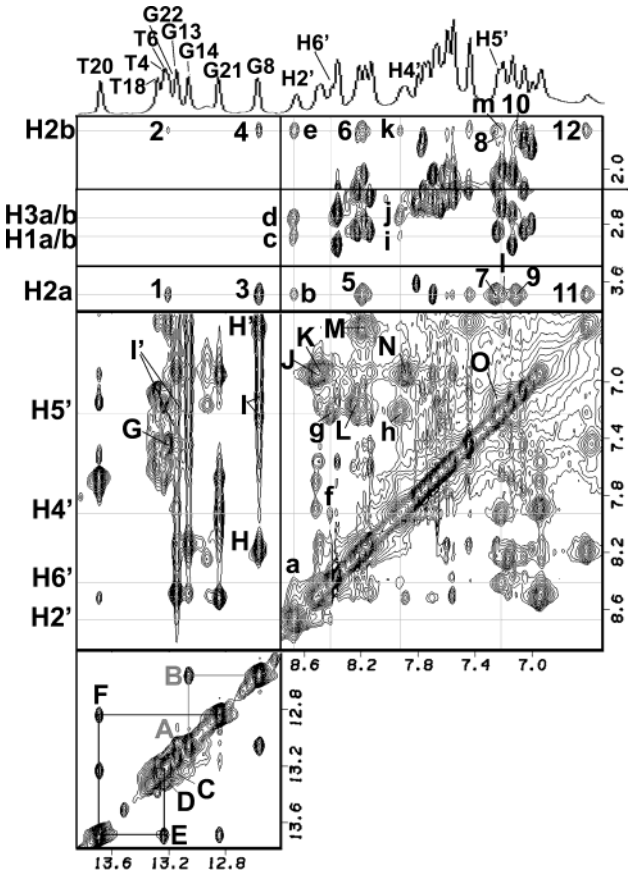

FIGURE 4: Expanded NOESY (150 ms mixing time) contour plots of the [POB]dG·dC 11mer duplex in H_2O buffer at 5 °C. The assignments of the 10 imino protons are given above the 1-D spectra (top). The NOE connectivities between adjacent base pairs in the symmetrical 12.4−14.0 ppm region are traced starting from dG13 located at one end of the helix and proceeding to dG14 located 3′ to [POB]dG7 (gray lines) and from dT6 located 5′ to [POB]dG7 and proceeding to G21 located at the other end of the helix (black lines). The connectivites between adjacent DNA imino protons are given by A, G13 to G14; B, G14 to G8; C, T6 to T18; D, T18 to T4; E, T4 to T20; and F, T20 to G21. The DNA−DNA cross-peaks indicating connectivites across the base pair are designated by G, dT6(NH3)-dA17(H2), and H,H′, dG8(NH1)-dC15(NH_2-4b,e). The cross-peaks between dG8 imino and dC16 aminos are designated by I and between T6 imino and C16 aminos by I′, indicating that the dC16 base is stacked within the helix. The cytosine hydrogen-bonded amino to exposed amino cross-peaks are indicated by J, dC2; K, dC10; L, dC11; M, dC15; N, dC1; and O, dC16. The intramolecular connectivities between POB protons (intersection of light gray lines) are designated by letters a−m. Their assignments are shown above the 1-D plot (top) and to the left of the contour plots: a−e, H2′ to H6′, H2a, H1a/b, H3a/b, and H2b, respectively; f and g, H6′ to H4′ and H5′, respectively; h−k, H4′ to H5′, H1a/b, H3a/b, and H2b, respectively; and l and m, H5′ to H2a and H2b, respectively. The cross-peaks 1−12 between DNA and POB protons are assigned as follows: 1, T6(NH3)-POB(H2a); 2, T6(NH3)-POB(H2b); 3, G8(NH1)-POB(H2a); 4, G8(NH1)-POB(H2b); 5, C15(NH4-b)-POB(H2a); 6, C15(NH4-b)-POB(H2b); 7, C16(NH4-1)-POB(H2a); 8, C16(NH4-1)-POB(H2b); 9, C16(NH4-2)-POB(H2a); 10, C16(NH4-2)-POB(H2b); 11, C15(NH4-e)-POB(H2a); and 12, C15(NH4-e)-POB(H2b).

of the [POB]dG7(H1′) to dG8(H8) step. The [POB]dG7-(H1′) resonance is very broad and overlaps with those for the H1′ protons of dT4, dG13, and dT20, as well as with that of the dC2(H5) proton. In addition, the dG8(H8) resonance overlaps with those of the H6 protons of dC2 and dC10. However, base to base connectivities are observed between the [POB]dG7(H8) proton and the flanking dG8-(H8) and dT6(H6) protons (peaks A and B, respectively, Figure 3), which is consistent with having the modified guanine stacked into the helix. The base to H1′ NOE connectivities for the complementary strand segment d(G14-C15-C16-A17-T18) (gray lines, Figure 3) can be followed without any disruptions. The minor groove dC16(H1′) resonance is shifted considerably downfield relative to the analogous resonance in the unmodified control duplex (Figures 3 and 5). The remaining chemical shift differences between the control and the modified duplexes for the nonexchangeable major groove and minor groove protons are summarized in Figure 5a,b, respectively, and in Table S6. In general, small chemical shift differences (<0.2 ppm) are observed, with the exception of dC16. In addition, to the H1′ proton (Δ ppm, −0.89), the chemical shifts for the H2′ and H2″ protons are also shifted downfield (Δ ppm, −0.22 and −0.26, respectively) relative to their values in the control duplex. The overall nonexchangeable proton NOE and chemical shift results are consistent with a minimally perturbed B-DNA duplex but with the minor groove edge of the dC16 sugar ring displaced slightly out of the helix and into the minor groove.

Cross-peak patterns involving base to sugar (NOESY) and sugar to sugar protons (NOESY and COSY) were qualitatively evaluated to differentiate between syn and anti glycosidic torsion angles (*25*) and between the C3′-endo and C2′-endo families of DNA sugar pucker conformations (*15*). Analysis of the proton NMR data establishes that all the residues, with the exception of the modified guanine, adopt anti glycosidic torsion angles with C2′-endo sugar pucker conformations. It was not possible to unambiguously determine these parameters for the [POB]dG7 residue because of the broad, weak, and overlapped NOE and COSY cross-peaks belonging to this residue. Previously, it has been established that DNA residues adopting syn glycosidic torsion angles with the C2′-endo sugar pucker conformations display up to 5 ppm downfield sugar C1′ carbon chemical shifts (*26*, *27*). Analysis of the ^{13}C-^{1}H HMQC spectrum of the [POB]dG·dC duplex adduct in D_2O buffer at 25 °C indicates that the [POB]dG7(C1′) chemical shift is similar to its value in the unmodified control duplex (Figure S2, Supporting Information). Interestingly, the C1′ chemical shifts of the dC15 and dC16 residues are shifted downfield by −1.25 and −0.96 ppm, respectively, suggesting that χ for these residues may be some intermediate value between an anti and a syn orientation (Figure S2).

The assignments for the exchangeable 10 imino protons in the modified duplex are shown above the 1-D spectrum of the [POB]dG·dC 11mer duplex in 9:1 H_2O:D_2O buffer at 5 °C in Figure 4. The tracing of the imino−imino NOE connectivities between adjacent base pairs indicates the presence of base pair stacking interactions starting from dG21 located at one end of the helix and proceeding to dT6 located 5′ to [POB]dG7 (black lines, Figure 4) and from dG8 located 3′ to [POB]dG7 and proceeding to dG13 located at the other end of the helix (gray lines, Figure 4). The discontinuity at the dT6-[POB]dG7-dG8 steps is due to[POB]dG7 no longer having an imino proton (Figure 1). However, NOEs can be observed between dC16 amino protons and the flanking dG8 and dT6 imino protons (peaks I and I′, respectively, Figure 4), indicating that dC16 is stacked into the helix. Furthermore, NOEs between dT6 and dG8 imino protons are not

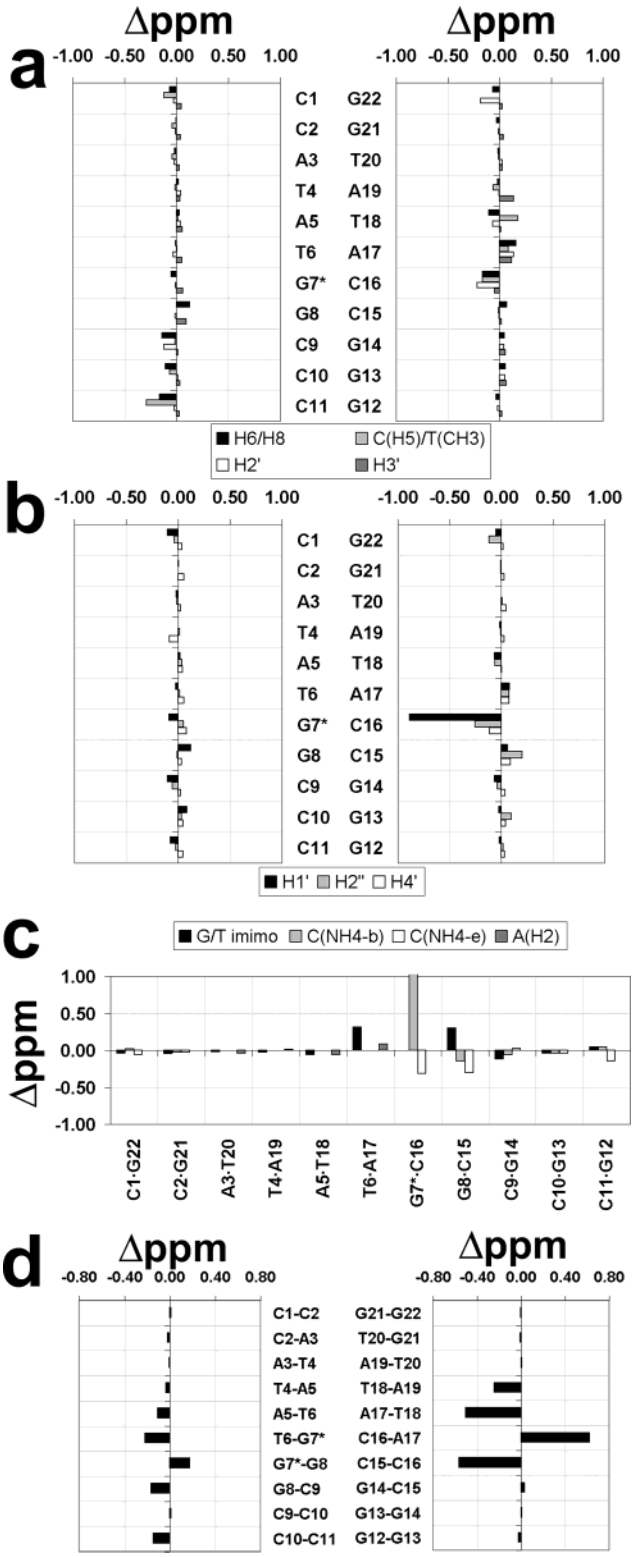

FIGURE 5: Summaries of proton and phosphorus chemical shift differences (Δ ppm) between control duplex and adduct duplex. A positive shift indicates an upfield shift relative to the control, while a negative value indicates a downfield shift. (a) Nonexchangeable H8/H6, cytosine H5/thymine methyl, and sugar H2′ and H3′ major groove protons. (b) Nonexchangeable sugar H1′, H2″, and H4′ minor groove protons. (c) Exchangeable G(NH1)/TNH3 imino, C(NH4) hydrogen-bonded amino, C(NH4) exposed amino, and A(H2). (d) Phosphorus.

observed, ruling out the possibility that the modified [POB]-dG7 and partner dC16 are looped out of the helix, and flanking dT6·dA17 and dG8·dC15 base pairs are stacked on each other. The flanking dT6 and dG8 imino protons are both shifted upfield by approximately 0.3 ppm relative to their values in the unmodified control duplex (Figure 5c and Table S6), while all the remaining imino protons exhibit similar chemical shifts relative to their values in the control duplex (Figure 5c).

The observed NOE patterns between the imino protons and the base and amino protons establish Watson−Crick base pairing at all dA·dT pairs (dT imino to dA(H2) across the pair) and at all dG·dC pairs (dG imino to dC aminos across the pair), with the exception of the modified base pair (Figure 4). The connectivity between the 5′-flanking dT6 imino proton and dA17(H2) is designated by peak G in Figure 4, while the connectivity between the 3′-flanking dG8 imino proton and the C15 hydrogen-bonded and exposed amino protons is designated by peaks H and H′, respectively, in Figure 4. One of the partner dC16 amino protons is shifted upfield by 1.12 ppm relative to the hydrogen-bonded amino proton in the control duplex, while the other is shifted downfield by −0.31 ppm relative to the exposed amino proton in the control duplex (broad peak O, Figures 4 and 5c). These differences in the dC16 amino protons' chemical shifts must reflect changes in the base stacking and hydrogen-bonding patterns of this residue in the modified duplex.

Phosphorus Resonances. The proton−phosphorus correlation spectra for the modified and control duplexes in D_2O buffer at 25 °C are shown in Figure S3 and the phosphorus chemical shift differences (control − modified) are summarized in Figure 5d. The largest chemical shift differences occur at the dC15-dC16 (−0.56 Δ ppm), dC16-dA17 (+0.62 Δ ppm), and dA17-T18 (−0.50 Δ ppm) steps in the complementary strand (Figure 5d). This pattern of downfield, upfield, downfield shifts centered about dC16 are mirrored, to a lesser degree, in the modified strand: dT6-[POB]dG7 (−0.22 Δ ppm), [POB]dG7-dG8 (+0.18 Δ ppm), and dG8-dC9 (−0.16 Δ ppm) steps centered about [POB]dG7. These results suggest that the effect of the distortion in the phosphodiester backbone at the dC16-dA17 and [POB]dG7-dG8 steps is opposite in direction to that of the flanking 5′ and 3′ steps.

POB Resonances. The intramolecular connectivities between the 10 POB protons are designated by the intersection of the light gray lines in both Figures 3 and 4 and by the letters a−n with their assignments shown above and to the left of the contour plots. The POB ligand proton and carbon chemical shifts are listed in Table S3.

Although the POB NOE cross-peaks are broad, exchange cross-peaks between two or more distinct types of conformations are not observed at the NMR time scale. The broad overlapped lines, however, made the assignment process challenging because the through bond connectivities for the aliphatic butyl chain protons could not be followed in the phase-sensitive COSY spectra at either 25 or 5 °C, although they were present but very weak in the TOCSY data sets. In addition, the chemical shift for POB(H2a) overlaps with those of C1(H5′/H5″), and the chemical shift for POB(H5′) overlaps with that of C15(H6) (Figures 3 and 4). The chemical shifts for the POB(H1a) and POB(H1b) protons are overlapped, as are the chemical shifts for the POB(H3a) and POB(H3b) protons (Figures 3 and 4). Despite broad line widths, the POB pyridyl ring protons, on the other hand, were readily assigned after analysis of the through bond

Table 1: DNA−POB NOE Distance Restraints as Compared to Distances in the 10 Structures of the [POB]dG·DC 11mer

	lower bound	upper bound	distance in structures (Å)
Nonexchangeable DNA Protons			
T6(CH_3)−POB(H2b)	3.00	5.00	3.65[a] ± 0.29
T6(CH_3)−POB(H2a)[4b]	3.00	5.00	5.19[a] ± 0.20
T6(CH_3)−POB(H2′)[1b]	4.50	6.00	5.70[a] ± 0.16
T6(H6)−POB(H2b)[2b]	4.50	6.00	5.65 ± 0.27
C15(H5)−POB(H2b)[3b]	3.30	5.00	4.91 ± 0.13
C15(H5)−POB(H2a)	3.30	5.00	3.55 ± 0.08
C15(H6)−POB(H2a)	4.50	6.00	4.86 ± 0.10
C15(H1′)−POB(H2a)	4.50	6.00	6.15 ± 0.12
T6(CH_3)−POB(H1a/H1b)	3.00	6.00	3.60[a] ± 0.30
T6(CH_3)−POB(H3a/H3b)	3.00	6.00	4.51[a] ± 0.31
Exchangeable DNA Protons			
T6(NH3)−POB(H2b)[2c]	3.80	5.50	4.48 ± 0.15
T6(NH3)−POB(H2a)[1c]	4.50	6.00	5.45 ± 0.05
G8(NH1)−POB(H2b)[4c]	4.50	6.00	5.45 ± 0.16
G8(NH1)−POB(H2a)[3c]	2.80	4.50	3.92 ± 0.21
C15(NH4-b)−POB(H2b)[6c]	3.30	5.00	4.43 ± 0.09
C15(NH4-b)−POB(H2a)[5c]	1.80	3.50	2.83 ± 0.05
C15(NH4-e)−POB(H2b)[12c]	3.80	5.50	4.28 ± 0.10
C15(NH4-e)−POB(H2a)[11c]	2.80	4.50	2.82 ± 0.05
C16(NH4-1)−POB(H2b)[8c]	1.80	3.50	2.53 ± 0.20
C16(NH4-1)−POB(H2a)[7c]	1.80	3.50	2.08 ± 0.12
C16(NH4-2)−POB(H2b)[10c]	1.80	3.50	2.70 ± 0.17
C16(NH4-2)−POB(H2a)[9c]	1.80	3.50	2.21 ± 0.05

[a] Averaged value; cross-peaks labeled 1b−4b and 1c−12c are designated in Figures 3 and 4, respectively.

COSY and TOCSY data and the through space NOESY data, suggesting that the carbonyl to pyridyl C3′ bond (ρ', Figure 1) retains some double bond characteristics and thus reduced motion.

POB−DNA Intermolecular NOEs. A total of 22 intermolecular NOE connectivities between the POB ligand and the DNA protons has been assigned in the NOESY spectra (300 ms mixing time in D_2O buffer, Figure 3, and 150 ms mixing time in H_2O buffer, Figure 4) at 5 °C (Table 1). Ten involve nonexchangeable major groove DNA protons. The POB-(H2a) and POB(H2b) protons are involved in three of these interactions with the 5′-flanking dT6 residue on the modified strand, predominately with the dT6 methyl group, and in four involving the 3′-flanking dC15 residue on the complementary strand, predominately with the dC15(H5) proton. These NOEs position the POB ligand in the major groove and are centered between the flanking dT6·dA17 and dG8·dC15 base pairs. An additional two intermolecular NOEs are observed between the POB(H1a/H1b) and POB(H3a/H3b) protons and the dT6 methyl group (Table 1). With the exception of one very weak NOE between the POB pyridyl ring H2′ proton and the dT6 methyl group (Figure 3, peak 1), all the NOE contacts are between butyl chain protons and DNA, suggesting that the pyridyl ring is not interacting significantly with the DNA. However, this one weak contact is still observed at a lower mixing time (150 ms) and thus provides an indication to a preference for the orientation of the ring nitrogen as being on the opposite side or trans to the carbonyl group (as shown in Figure 2a−c). In agreement, the NOE cross-peaks between the POB H2a/H2b protons and pyridyl ring protons are stronger with POB(H2′) (peaks b and e, Figure 3) than with POB(H4′) (peaks i and j, Figure 3) located on the opposite side of the ring.

An additional 12 intermolecular NOEs are between exchangeable DNA protons and POB (Figure 4 and Table 1) and further define the position of the POB ligand with respect to the surrounding DNA residues. Both flanking dT6 and dG8 imino protons show weak to medium NOEs to the POB H2a and H2b protons (peaks 1−4, Figure 4 and Table 1). Medium to strong NOEs are observed between the major groove amino protons of dC16 (peaks 7−10, Figure 4) and dC15 (peaks 5, 6, 11, and 12, Figure 4) and the H2a and H2b protons of POB.

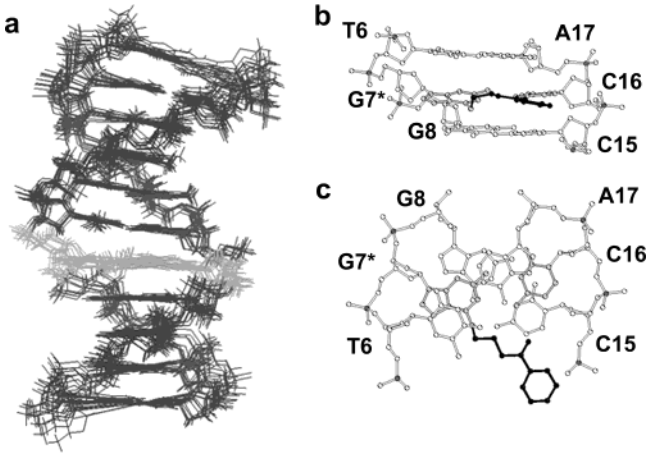

FIGURE 6: (a) Superposition of 10 structures of the [POB]dG·dC 11mer adduct duplex calculated using the program DUPLEX. The [POB]dG7·dC16 base pair is shown in gray. Views of the d(T6-[POB]dG7-G8) three base pair segment of the lowest energy structure looking (b) into the major groove and normal to the helix axis and (c) down the helix axis. The modified [POB]G6·C17 base pair is gray, and the POB ligand is black.Panels b and c were generated using Molscript VI.1 (*21*).

The NMR data indicate that the aromatic POB pyridyl ring is extended out into the major groove away from the DNA rather than pointing in and intercalating into the DNA. NOEs could be not be detected between the four POB pyridyl ring protons (H2′, H4′, H5′, and H6′) and the exchangeable imino or amino protons in the d(T6-[POB]dG7-dG8)·d(C15−C16-A17) segment.

Structure Determination of the [POB]dG·DC 11mer. A set of 22 POB−DNA (Table 1), five POB−POB, and 271 DNA−DNA unambiguous NOE cross-peaks has been identified for conversion into NOE distance restraints. The program DUPLEX (as described in the Materials and Methods) was used to calculate the structures of the adduct duplex. Ten of the structures, which exhibit the lowest energies (−484.44 ± 9.16 kcal/mol) and best fit to the NMR data, are shown superimposed in Figure 6a. RMS deviation for all heavy atoms is 1.03 ± 0.28 Å (Table 2). The statistical analyses of the structures are summarized in Table 2. A stereoview looking in the major groove of the lowest energy structure is shown in Figure 7a.

Views looking into the major groove and normal to the helical axis (Figure 6b) and down the helix axis (Figure 6c) of the central three base pair segment of the lowest energy structure show that the pyridyl ring is extended away from the DNA and that the POB ligand is in the plane of the [POB]-dG7·dC16 base pair. The POB ligand is positioned toward the center of the major groove and away from the phosphodiester backbone. The modified guanine and partner cytosine residues are stacked into the helix with the glycosidic torsions in anti orientations (χ = 239.9 ± 8.7 and χ = 241.6 ± 2.9°, respectively), in agreement with the NMR data

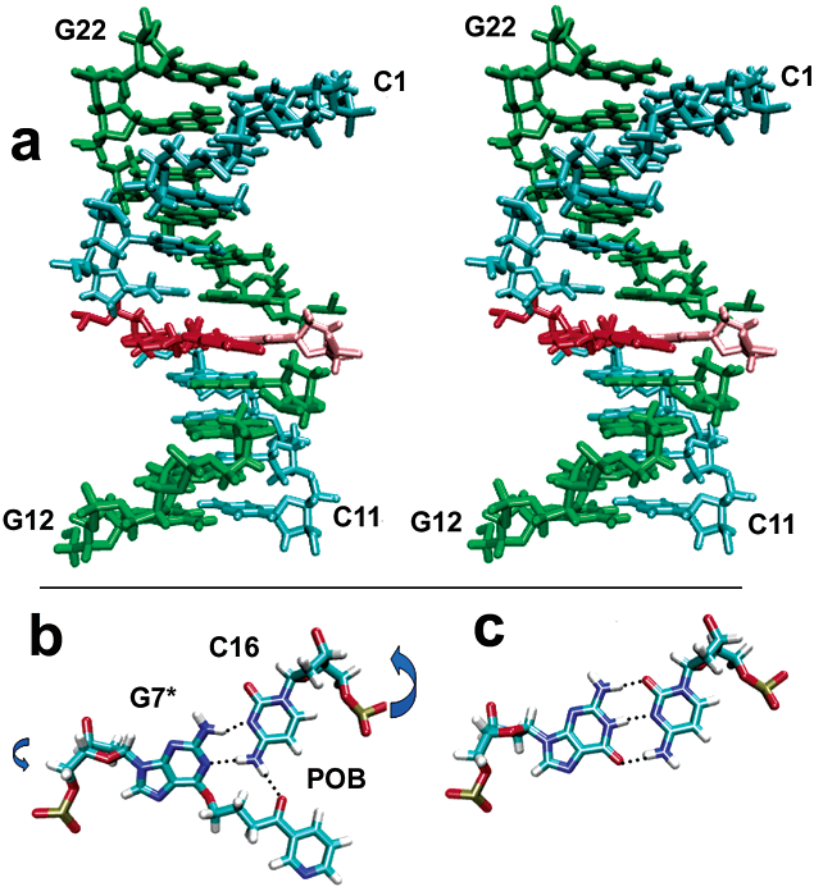

FIGURE 7: (a) Stereoview looking in the major groove of the lowest energy structure with the modified strand (C1-C11) in blue, complementary strand (G12-G22) in green, [POB]dG7 in red, and dC16 in pink. The terminal residues are labeled. (b) The bases of the modified guanine, partner cytosine, and POB pyridyl ring form a triplex through an unusual hydrogen-bonding pattern (dashed lines). To accommodate the larger aromatic surface area while still retaining the normal overall dimensions of the DNA helix, the phosphate backbone at the dC16-dA17 step, and to a lesser degree, the [POB]dG7-G8 twist (arrows), in agreement with the phosphorus chemical shift differences (Figure 5d). (c) The dG7·dC16 base pair in the control DNA duplex is shown for comparison.

Table 2: Experimental NMR Data and Statistics for the 10 Best Structures of the [POB]dG·DC 11mer Duplex Adduct

total no. of unambiguous restraints	325
NOE POB−POB	5
NOE POB−DNA exchangeable protons	12
NOE POB−DNA nonexchangeable protons	8
NOE DNA−DNA intraresidue	
strand 1	81
strand 2	74
NOE DNA−DNA interresidue	
strand 1	64
strand 2	52
hydrogen bonds	29
total number of violations	16
> 0 < 0.05	6
> 0.05 < 0.1	5
> 0.1 < 0.25	4
> 0.25 < 0.5	1
>0.5	0
RMSD (heavy atoms, pair wise 10 structures)	1.03 ± 0.28
family 1	0.68 ± 0.18
family 2	0.75 ± 0.20
energies: all 10 structures	−484.4 ± −9.2
family 1	−488.7 ± 3.6
family 2	−480.1 ± 11.3

(Table S7). The comparisons of the base stacking interactions between the modified and the control duplexes at the d([POB]G7-G8)·d(C15-C16) and d(T6-[POB]G7)·d(C16-A17) dimer steps are shown in Figure S4, Supporting Information. Relative to the 5′ and 3′ flanking base pairs, the cytosine in the modified base pair slides slightly into the minor groove.

The 10 structures can be further subdivided into two subsets of families, and each family is defined by the torsion angles α′ and β′ at the POB-O^6-dG7 linkage site (Figure S5, Supporting Information). Family 1 is comprised of five structures having the lowest energy (−488.73 ± 3.84 kcal/mol), best goodness of fit to the NMR data, and pair wise RMSD value of 0.68 ± 0.18 (heavy atoms). In these structures, the POB-O^6-dG7 bond is directed ∼ 90° on the 5′ side of the modified G with α′ 94.2 ± 1.3 and β′ 260.2 ± 0.8° (Figure S5). Family 2 is also comprised of five structures but has higher energy (−480.14 ± 11.31 kcal/mol), lower fit to the NMR data, and a slightly higher pair wise RMSD of 0.75 ± 0.20. The POB-O^6-dG7 bond is directed ∼ 90° on the 3′ side of the modified G, with α′ 293.4 ± 1.3 and β′ 103.2 ± 0.5°. Both families are consistent with the NMR data and may reflect the motional flexibility of the POB ligand with respect to the modified guanine. This possible rotation about α′ and β′ can also explain, in part, the broad line widths obtained for the POB ligand and modified base pair.

The modified base pair adopts a wobble base pairing scheme similar to the one shown schematically in Figure 2c (Figure 7b). The POB pyridyl ring together with the bases of the modified guanine and cytosine residues form a triplex

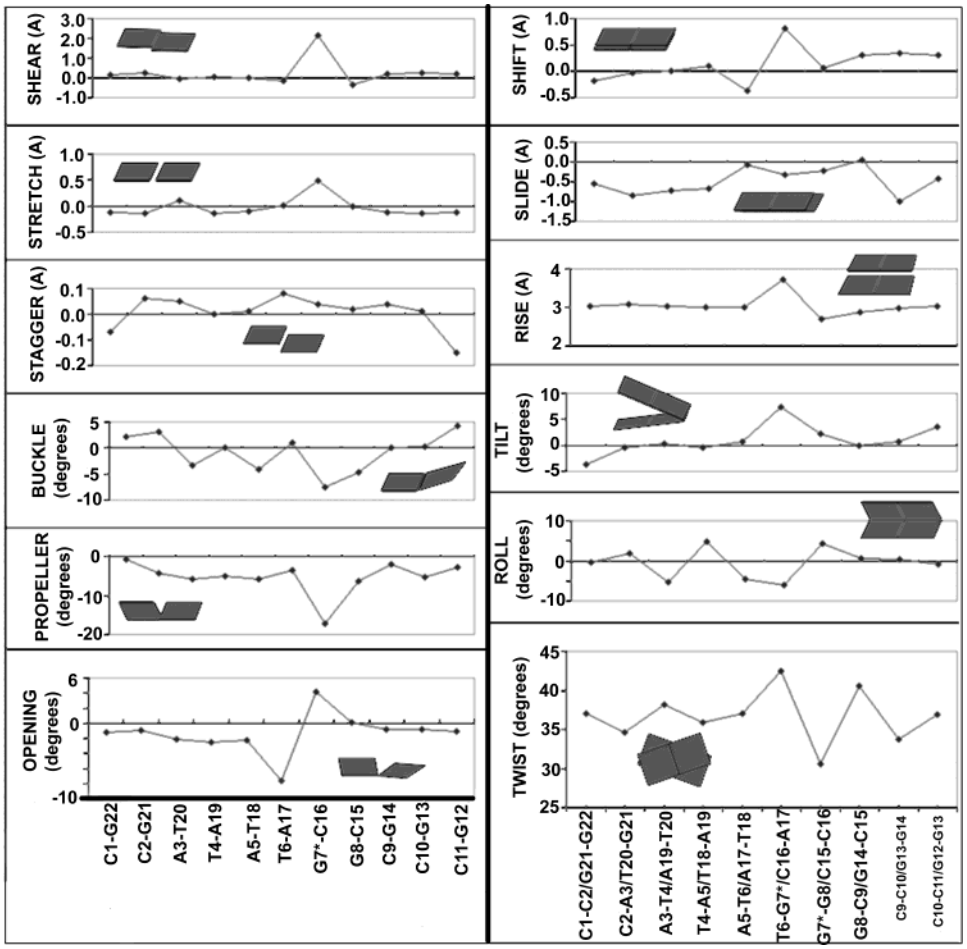

FIGURE 8: Comparative analysis of local base pair (left) and dimer step (right) parameters (see schematic insets for definitions) of the [POB]dG.dC 11mer duplex. Values were calculated using the nucleic acid structure analysis program 3DNA (*19*, *20*).

through an unusual hydrogen-bonding pattern that includes one between the POB carbonyl oxygen and the dC16 amino proton (Figure 7b). The latter hydrogen bond is consistent with the −0.31 downfield chemical shift of the dC16 amino proton relative to its value in the control duplex (Figure 5b).

Helical Parameters. Comparative analyses of local base pair and dimer step helical parameters for the lowest energy [POB]dG·dC 11mer duplex structure are shown in Figure 8. Significant distortions in the modified base pair due to the wobble base pairing and POB adduct include shearing, propeller twisting, and opening (Figure 8). These distortions are in agreement with the UV melting results, which show that the POB adduct destabilizes the helix significantly by a 17.6 °C decrease in melting temperature relative to the control duplex (Figure S1).

An average twist angle between base pair dimer steps is approximately 36°. The dT6·dA17 to [POB]dG7·dC16 dimer step is overtwisted (42.5°), while the dG8·dC15 to [POB]-dG7·dC16 dimer step is undertwisted (30.6°) (Figure 8). The twist angle is again overwound at the dG8·dC15 to dC9·dG14 dimer step (40.5°) (Figure 8). This pattern of over-under-overtwisting for the d(T6-[POB]G7-G8-C9)·d(G14-C15−C16-A17) segment is in complete agreement with the large phosphorus chemical shift differences observed for the residues around the POB adduction site (Figure 5d). The twisting of the phosphodiester backbone around the modified base pair with respect to the flanking base pairs maximizes base stacking interactions. The subsequent changes in the stacking patterns with flanking dT6·dA17 and dG8·dC15 base pairs explain the small ∼0.3 Δ ppm upfield chemical shifts differences observed for the dT6 and dG8 imino protons (Figure 5c). The [POB]dG7·dC16 base pair shifts slightly toward the major groove relative to the dT6·dA17 base pair (−0.37 Å) and to a larger degree toward the minor groove relative to the dG8·dC15 base pair (+0.81 Å) (Figures 7b and 8). The displacement of the dC16 residue slightly into the minor groove is in agreement with the large downfield chemical shift difference for the dC16(H1′) proton (Figure 5a).

Biological Implications. The covalent binding of a bulky alkylating agent such as POB to DNA can alter biological processing of the DNA by cellular proteins governing replication, transcription, and repair and thereby cause mutations and ultimately cancer, especially if the lesion is located in an oncogene or tumor suppressor gene (*28*, *29*). Consequently, considerable efforts are being made to understand how adduct conformation affects cellular responses to DNA damage. Our studies show that the POB ligand is located in the major groove, parallel with the modified base pair, with the ligand oriented toward the center of the groove. The modified guanine base, partner cytosine base, and POB pyridyl ring in the [POB]dG·dC 11mer adduct duplex form a novel triplex through an unusual hydrogen-bonding pattern. The modified base pair adopts wobble hydrogen bonding due to no longer having an imino proton available as a hydrogen donor. The two hydrogen bonds present across the

[POB]dG7 and dC16 base pair are between the [POB]dG-(N1) nitrogen and the dC(NH4) amino proton and between the [POB]dG(NH2) amino proton and the dC(N3) nitrogen. An additional hydrogen bond appears to be present between the POB carbonyl oxygen and the second dC16 amino proton. The POB modification induces undertwisting at the lesion site and a subsequent overtwisting at the flanking steps, predominately on the complementary strand. As a result, the partner cytosine slides slightly into the minor groove to maximize stacking interactions between the modified base pair and the flanking base pairs. The distortions induced in the modified duplex by the POB adduct result in a significant decrease in the melting temperature of 17.6 °C.

The destabilization of the helix, altered hydrogen-bonding properties of the modified guanine, and twisting of the phosphodiester backbone would be expected to be important factors in the recognition of the POB damaged DNA by repair proteins. In addition, these distortions provide clues as to why thymine rather than cytosine is found preferentially incorporated across the [POB]dG adduct during replication (*6*). Previous studies on the structures of the O^6meG and O^6etG adducts located in DNA duplexes indicate that the O^6-alkyl dG·dT base pair can adopt a Watson−Crick-like conformation with minimal distortion to the helix, while an O^6-alkyl dG·dC base pair results in greater distortions and can exhibit dynamic equilibrium among various conformations (Figure 2) (*7*, *8*). The data presented here on the structure of the [POB]dG·dC duplex adduct are in agreement with this previous work. The alterations from normal pairing can result in poor accommodation of the POB modified dG·dC pair within the active site of a polymerase. Both replicative and bypass polymerases share a structural similarity in the vicinity of the active site, namely, an open pocket on the major groove side of the template (*30*). Previous studies indicate that this pocket can accommodate bulky adducts (*31*). The bulky POB group, which is located in the major groove side of the modified base, could possibly fit into a polymerase's open pocket, but the slight displacement of the cytosine residue into the minor groove and subsequent twisting of the phosphodiester backbone can potentially cause less than ideal accommodation of the nascent base pair in the active site. Studies currently underway in our laboratories on the structure of the [POB]dG·dT duplex adduct should shed further light on this subject.

ACKNOWLEDGMENT

This work was performed under the auspices of the U.S. Department of Energy by the University of California, Lawrence Livermore National Laboratory under Contract W-7405-Eng-48 and by Oak Ridge National Laboratory, managed by UT-Battelle, for the U.S. DOE under Contract DE-AC05-00OR22725. We thank Dr. T. Andrew Taton in the Department of Chemistry, University of Minnesota for access to his UV−vis spectrophotometer for the melting temperature experiments.

SUPPORTING INFORMATION AVAILABLE

Eight tables with the following information: partial charges for the O^6-dG-POB residue, torsion angle barriers for the POB ligand used in structure calculations, POB proton and carbon chemical shifts, nonexchangeable DNA proton and phosphorus chemical shifts, exchangeable DNA proton chemical shifts, chemical shift differences, DNA sugar pseudorotation (P) and glycosidic (χ) torsion angles, and POB dihedral angles. Five figures with the following information: melting curves, C1′ to H1′ expanded region of the natural abundance ^{13}C-^{1}H HMQC spectrum, proton-phosphorus HETCORR spectra for the modified and control duplexes, base stacking interaction comparisons between the modified and the control, and a description of the two subfamilies of structures. This material is available free of charge via the Internet at http://pubs.acs.org.

REFERENCES

1. Margison, G. P., and Santibanez-Koref, M. F. (2002) *BioEssays 24*, 255−66.
2. Hecht, S. S. (1998) *Chem. Res. Toxicol. 11*, 559−603.
3. Wang, L. J., Spratt, T. E., Liu, X. K., Hecht, S. S., Pegg, A. E., and Peterson, L. A. (1997) *Chem. Res. Toxicol. 10*, 562−7.
4. Wang, L. J., Spratt, T. E., Pegg, A. E., and Peterson, L. A. (1999) *Chem. Res. Toxicol. 12*, 127−31.
5. Thomson, N. M., Kenney, P. M., and Peterson, L. A. (2003) *Chem. Res. Toxicol. 16*, 1−6.
6. Pauly, G. T., Peterson, L. A., and Moschel, R. C. (2002) *Chem. Res. Toxicol. 15*, 165−9.
7. Sriram, M., van der Marel, G. A., Roelen, H. L., van Boom, J. H., and Wang, A. H. (1992) *Biochemistry 31*, 11823−34.
8. Sriram, M., van der Marel, G. A., Roelen, H. L., van Boom, J. H., and Wang, A. H. (1992) *EMBO J. 11*, 225−32.
9. Ginell, S. L., Kuzmich, S., Jones, R. A., and Berman, H. M. (1990) *Biochemistry 29*, 10461−5.
10. Williams, L. D., and Shaw, B. R. (1987) *Proc. Natl. Acad. Sci. U.S.A. 84*, 1779−83.
11. Patel, D. J., Shapiro, L., Kozlowski, S. A., Gaffney, B. L., and Jones, R. A. (1986) *Biochemistry 25*, 1027−36.
12. Patel, D. J., Shapiro, L., Kozlowski, S. A., Gaffney, B. L., and Jones, R. A. (1986) *J. Mol. Biol. 188*, 677−92.
13. Sklenar, V., Miyashiro, H., Zon, G., Miles, H. T., and Bax, A. (1986) *FEBS Lett. 208*, 94−8.
14. Bax, A., and Subramanian, S. (1986) *J. Magn. Reson. 67*, 565−70.
15. Van de Ven, F. J., and Hilbers, C. W. (1988) *Eur. J. Biochem. 178*, 1−38.
16. Arnott, S., Bond, P. J., Selsing, E., and Smith, P. J. (1976) *Nucleic Acids Res. 3*, 2459−70.
17. Cosman, M., Hingerty, B. E., Geacintov, N. E., Broyde, S., and Patel, D. J. (1995) *Biochemistry 34*, 15334−50.
18. Frisch, M. J.; Trucks, G. W.; Schlegel, H. B.; Scuseria, G. E.; Robb, M. A.; Cheeseman, J. R.; Zakrzewski, V. G.; Montgomery, J. A., Jr.; Stratmann, R. E.; Burant, J. C.; Dapprich, S.; Millam, J. M.; Daniels, A. D.; Kudin, K. N.; Strain, M. C.; Farkas, O.; Tomasi, J.; Barone, V.; Cossi, M.; Cammi, R.; Mennucci, B.; Pomelli, C.; Adamo, C.; Clifford, S.; Ochterski, J.; Petersson, G. A.; Ayala, P. Y.; Cui, Q.; Morokuma, K.; Malick, D. K.; Rabuck, A. D.; Raghavachari, K.; Foresman, J. B.; Cioslowski, J.; Ortiz, J. V.; Stefanov, B. B.; Liu, G.; Liashenko, A.; Piskorz, P.; Komaromi, I.; Gomperts, R.; Martin, R. L.; Fox, D. J.; Keith, T.; Al-Laham, M. A.; Peng, C. Y.; Nanayakkara, A.; Gonzalez, C.; Challacombe, M.; Gill, P. M. W.; Johnson, B. G.; Chen, W.; Wong, M. W.; Andres, J. L.; Head-Gordon, M.; Replogle, E. S.; Pople, J. A. *Gaussian 98*; Gaussian, Inc.: Pittsburgh, PA, 1998.
19. Lu, X.-J., and Olson, W. K. (2003) *Nucleic Acid Res. 31*, 5108−21.
20. Olson, W. K., Bansal, M., Burley, S. K., Dickerson, R. E., Gerstein, M., Harvey, S. C., Heinemann, U., Lu, X.-J., Neidle, S., Shakked, Z., Sklenar, H., Suzuki, M., Tung, C.-S., Westhof, E., Wolberger, C., and Berman, H. M. (2001) *J. Mol. Biol. 313*, 229−37.
21. Kraulis, P. J. (1991) *J. Appl. Crystallogr. 24*, 946−50.
22. Gaffney, B. L., Marky, L. A., and Jones, R. A. (1984) *Biochemistry 23*, 5686−91.
23. Hare, D. R., Wemmer, D. E., Chou, S. H., Drobny, G., and Reid, B. R. (1983) *J. Mol. Biol. 171*, 319−36.
24. Wuthrich, K. (1986) *NMR of Proteins and Nucleic Acids*, John Wiley & Sons, New York.

25. Patel, D. J., Kozlowski, S. A., Nordheim, A., and Rich, A. (1982) *Proc. Natl. Acad. Sci. U.S.A. 79*, 1413−7.
26. Ghose, R., Marino, J. P., Wiberg, K. B., and Prestegard, J. H. (1994) *J. Am. Chem. Soc. 116*, 8827−8.
27. Greene, K. L., Wang, Y., and Live, D. (1995) *J. Biomol. NMR 5*, 333−8.
28. Garner, R. C. (1998) *Mutat. Res. 402*, 67−75.
29. Perera, F. P., and Weinstein, I. B. (2000) *Carcinogenesis 21*, 517−24.
30. Kunkel, T. A., and Bebenek, K. (2000) *Annu. Rev. Biochem. 69*, 497−529.
31. Perlow, R. A., and Broyde, S. (2001) *J. Mol. Biol. 309*, 519−36.

BI035217V